The Astrophysical Journal, 916:74 (12pp), 2021 August 1 https://doi.org/10.3847/1538-4357/ac0537

A Photoionization Mass Spectrometry Investigation into Complex Organic Molecules Formed in Interstellar Analog Ices of Carbon Monoxide and Water Exposed to Ionizing Radiation

Andrew M. Turner[1,2], Alexandre Bergantini[1,2], Andreas S. Koutsogiannis[1,2], N. Fabian Kleimeier[1,2], Santosh K. Singh[1,2], Cheng Zhu[1,2], André K. Eckhardt[3], and Ralf I. Kaiser[1,2]
[1] Department of Chemistry, University of Hawaii at Manoa, Honolulu, HI 96822, USA; ralfk@hawaii.edu
[2] W. M. Keck Laboratory in Astrochemistry, University of Hawaii at Manoa, Honolulu, HI 96822, USA
[3] Department of Chemistry, Massachusetts Institute of Technology, Cambridge, MA 02139, USA
Received 2021 April 9; revised 2021 May 19; accepted 2021 May 20; published 2021 July 29

Abstract

The formation of complex organic molecules by energetic electrons mimicking secondary electrons generated within trajectories of galactic cosmic rays was investigated in interstellar ice analog samples of carbon monoxide and water at 5 K. Simulating the transition from cold molecular clouds to star-forming regions, newly formed products sublimed during the temperature-programmed desorption and were detected utilizing isomer-specific photoionization reflectron time-of-flight mass spectrometry. Using isotopically labeled ices, tunable photoionization, and adiabatic ionization energies to discriminate between isomers, isomers up to $C_2H_4O_2$ and $C_2H_6O_2$ were identified, while non-isomer-specific findings confirmed complex organics with molecular formulas up to $C_4H_6O_4$. The results provide important constraints on reaction pathways from simple inorganic precursors to complex organic molecules that have both astrochemical and astrobiological significance.

Unified Astronomy Thesaurus concepts: Laboratory astrophysics (2004); Interdisciplinary astronomy (804); Interstellar molecules (849); Astrochemistry (75)

1. Introduction

Complex organic molecules (COMs), defined in astronomy as organic compounds with six or more atoms, serve as evidence for the advanced chemistry possible in the cold confines of the interstellar medium (ISM). With densities of 10^2–10^4 molecules cm^{-3}, temperatures of 10–15 K, and efficient shielding of visible and ultraviolet photons, it is remarkable that cold molecular clouds can operate as natural molecular factories toward the formation of COMs (Kaiser 2002). Nevertheless, astronomical observations combined with laboratory studies and computational models indicate that these molecular clouds play a key role in the formation of COMs, which comprise nearly 80% of the more than 200 interstellar molecules detected thus far (Zamirri et al. 2019; Turner & Kaiser 2020; Woon 2021). In these molecular clouds, interstellar dust particles coated with an icy mantle of simple compounds such as water (H_2O), carbon monoxide (CO), carbon dioxide (CO_2), methane (CH_4), formaldehyde (H_2CO), ammonia (NH_3), and methanol (CH_3OH; Boogert et al. 2015) serve as chemical focal points for the formation of new organics by ionizing radiation such as galactic cosmic rays (GCRs) or the internal ultraviolet photon field (Mehringer & Snyder 1996). Ionizing radiation creates secondary electrons, atoms, molecules, and radicals that can be vibrationally excited (Abplanalp et al. 2016), electronically excited (Zhou et al. 2010), or possess excess kinetic energy (Morton & Kaiser 2003) that allows for nonequilibrium chemistry capable of overcoming reaction barriers (Kaiser 2002). Various processes such as grain explosions can eject newly formed molecules into the gas phase at 10 K (d'Hendecourt et al. 1982; Tielens et al. 1994; Westley et al. 1995; Kaiser et al. 1997; Vasyunin & Herbst 2013); alternatively, the molecules can remain in the icy mantles to sublime as the cold molecular cloud transits to star-forming regions (He et al. 2018). While this process—radiation-induced chemistry of interstellar ices providing more complex molecules to the gas phase—represents a foundation for the assortment of COMs detected in the ISM, the precise reaction pathway for each individual COM remains largely elusive. Although organic reactants such as methane or methanol signify a reasonable basis for COMs, water is the most abundant molecule in interstellar and cometary ices while carbon monoxide is one of the next most abundant molecules with observed column densities up to 26% relative to water toward molecular clouds and 30% relative to water in comets (Boogert et al. 2015). Carbon dioxide has similar abundances to carbon monoxide, while methanol, which has a similar interstellar abundance but only a fraction of the cometary abundance compared to carbon monoxide, is the only organic compound in appreciable amounts comparable to its inorganic neighbors. Analogous to Friedrich Wohler's famous 1828 synthesis of organic urea from inorganic ammonium cyanate (Keen 1984), the interstellar complex *organic* molecules may be formed from predominantly *inorganic* ices.

To investigate the degree to which inorganic precursors can produce COMs under interstellar conditions, we report on the facile synthesis of COMs in interstellar ice analogs of water and carbon monoxide. Previous studies of CO: H_2O ices have been performed, but with varying objectives and success. Bennett et al. (2011) attempted to identify COMs but were limited by infrared spectroscopy and quadrupole mass spectrometry (QMS) to the detection of formic acid (HCOOH). In other cases, characterization of the pristine CO: H_2O ice utilizing infrared spectroscopy was the primary objective with less concern for potential reaction products (Sandford et al. 1988; Devlin 1992; Jenniskens et al. 1995; Palumbo 1997; Collings et al. 2003; Zamirri et al. 2018). Adsorption of CO onto water ice (Al-Halabi et al. 2004) and the diffusion of hydrogen atoms into CO: H_2O ices leading to the hydrogenation of carbon monoxide to formaldehyde and methanol has been investigated (Awad et al. 2005; Petrik et al. 2014; Tsuge et al. 2020), but these hydrogenation reactions alone cannot

explain larger COMs in interstellar ices. To accomplish this, the present study utilizes energetic electrons to simulate secondary electrons caused by the interactions of GCRs to initiate the nonequilibrium chemistry leading toward COMs. Reflectron time-of-flight mass spectrometry is used as a more sensitive, isomer-selective technique than the QMS residual gas analyzers used in traditional space simulation experiments. While the 70–100 eV electron impact from a QMS can extensively fragment products, photoionization (PI) utilizing 8–11 eV photons was employed with the ReTOF-MS that can softly ionize the subliming products as the irradiated ices are heated from 5 K to room temperature. Because photons are tunable, photon energies can be chosen that allow for isomer-specific ionization and detection using known ionization energies. Using this PI-ReTOF-MS technique, the ability to form COMs from simple inorganic precursors of carbon monoxide and water was investigated under simulated conditions mimicking exposure of interstellar ices at typical lifetimes of molecular clouds of 10^6 yr. Results from these experiments expand astrochemical knowledge and provide evidence of formation pathways that lead to COMs in interstellar ice that not only can be brought into the gas phase, but can also become incorporated into comets and meteorites capable of delivering these COMs to worlds such as the early Earth.

2. Experimental

Experiments were performed in a stainless steel ultra-high vacuum chamber evacuated to pressures of a few 10^{-11} Torr (Jones & Kaiser 2013; Turner & Kaiser 2020). Ices of carbon monoxide (CO, 99.99%, Sigma Aldrich; ^{13}CO, 99% ^{13}C, Sigma Aldrich; C^{18}O, 95% ^{18}O, Sigma Aldrich) and water (H_2O, HPLC, Fisher; D_2O, 99.9% D, Sigma Aldrich; $H_2^{18}O$, 99% ^{18}O, Sigma Aldrich) were prepared by delivering premixed carbon monoxide and water (introduced after a triple freeze/thaw purification) via a glass capillary array to a polished silver target cooled to 5.0 ± 0.2 K to create a well-mixed, amorphous ice layer. The ice thicknesses were determined by exploiting laser interferometry (Turner et al. 2015) using the 632.8 nm output of a helium-neon laser. Typical ice thickness was 1000 nm, with the thinnest ice measuring 800 ± 200 nm. The ices were isothermally irradiated with 5 keV electrons to initiate reactions and monitored online and in situ using Fourier-transform infrared spectroscopy (Nicolet 6700, 4 cm^{-1} resolution). Utilizing the CASINO program (Hovington et al. 1997), 90% of the irradiated electron energy was deposited at 420 nm, while 99% was deposited at 600 nm (Figure 1), which is less than the ice thickness and ensures that the electrons only process the ice and not the substrate. While the average penetration depth of the electrons was 330 nm, 50% of the energy was deposited in the uppermost 160 nm. Doses ranged from 5 to 17 eV molecule^{-1}, which is consistent with the lifetime of a typical molecular cloud of 10^6 yr (Kaiser 2002). Using the integrated infrared absorption coefficients of CO (ν_1, 2138 cm^{-1}, 1.1×10^{-17} cm molecule^{-1}), ^{13}CO (ν_1, 2090 cm^{-1}, 1.3×10^{-17} cm molecule^{-1}), and H_2O (ν_2, 1660 cm^{-1}, 9.8×10^{-17} cm molecule^{-1}; (ν_1/ν_3, 3300 cm^{-1}, 3.8×10^{-16} cm molecule^{-1}; Bouilloud et al. 2015; Turner et al. 2018), the typical CO: H_2O ice ratio was found to be $1.0 \pm 0.4 : 1$, which serves as a suitable analog for inorganic ices in extraterrestrial environments. An analysis of infrared assignments in these irradiated ices has been reported previously (Bennett et al. 2011). Details of each experiment can be found in Table 1. After irradiation, the ices were warmed from 5 to 300 K at 1 K minutes^{-1} using a temperature-programmed desorption scheme (TPD). The subliming molecules were photoionized and detected by a reflectron time-of-flight mass spectrometer (ReTOF-MS; Jordon TOF Products, Inc.) to correlate the arrival times of the ions to mass-to-charge ratios (m/z) using the signal of a fast preamplifier (Ortec 9305) and a 4 ns bin width triggered at 30 Hz (Quantum Composers 9518). Experiments were also repeated with isotopically labeled reactants to confirm the assignment of the chemical formulas; the photoionization energy was tuned to discriminate isomers based on distinct ionization energies. The CO: H_2O ices utilized 10.82 eV (Ice 1), 10.49 eV (Ice 2), 10.23 eV (Ice 3), 9.75 eV (Ice 4), and 9.10 eV (Ice 5) photon energies, while CO: D_2O ices used 10.82 eV (Ice 6), 10.49 eV (Ice 7), and 10.23 eV (Ice 8). Ices of ^{13}CO: H_2O (Ice 9), ^{13}CO: D_2O (Ice 10), and C^{18}O: $H_2^{18}O$ (Ice 11) were repeated at 10.82 eV. These isotopically labeled ices were used to confirm the assigned formulas. To generate these photon energies, two pulsed Nd:YAG lasers (neodymium yttrium aluminum garnet, Spectra Physics, Quanta Ray PRO-250, 30 Hz) pumped two dye lasers (Sirah) and their outputs combined using difference resonant four-wave mixing ($\omega_{VUV} = 2\omega_1 - \omega_2$) with either krypton or xenon used as the nonlinear medium (Table 2; Hilbig & Wallenstein 1982). For 10.49 eV, the third harmonic (355 nm) of the Nd:YAG underwent frequency tripling by nonresonant four-wave mixing ($\omega_{VUV} = 3\omega_1$) using xenon. A blank experiment was performed without electron irradiation to verify that an external source of irradiation is necessary to generate the products.

3. Results

The following results describe the TPD profiles of the PI-ReTOF-MS analysis (Figure 2) in order of increasing mass-to-charge ratio of the products. Only compounds with formulas confirmed by isotopic labeling are included. Unless otherwise stated, evaluated ionization energies are obtained from the National Institute of Standards and Technology (NIST) Chemistry WebBook (Lias 2015). In general, the signal intensities decrease as the photon energy is lowered, which is expected as ionization cross sections similarly decrease. Thus, the absolute signals cannot be compared between profiles of different photon energies, but the profiles can be qualitatively compared or scaled until similar intensities are displayed. While small changes to intensity occur between ices of the same photon energy, but different isotopic labelings that do not affect the analysis, Ice 10 (^{13}CO: D_2O) presented consistently lower signals that occasionally were not above baseline. In these cases, Ice 10 was not utilized for confirmation.

H_2CO

The lowest mass product observed is H_2CO ($m/z = 30$), belonging to formaldehyde (Figure 3, left). The TPD profile shows a sharp peak at 160 K associated with the sublimation of the water matrix indicating that H_2CO co-sublimes with water, and a second, broad peak at 198 K with a shoulder at 214 K appears. A signal is only seen at 10.82 eV. The evaluated ionization energy of 10.88 ± 0.01 eV for formaldehyde proposes that formaldehyde should not be observed at 10.82 eV; however, the photoelectron spectrum by Niu et al. (1993) displayed a signal down to 10.85 eV while the photoelectron spectrum from von Niessen et al. (1980) suggests an adiabatic ionization energy of 10.7 eV. In addition, an inherent electric field effect of the experimental apparatus effectively reduces the ionization energy of sublimed molecules by up to 0.03 eV (Bergantini et al. 2018a), and previous studies have demonstrated that co-sublimation with water can affect the ionization energy of a molecule (Belau et al. 2007;

Table 1
Experimental Parameters of the Ices, Composition, Thickness, Irradiation Dose, and Photon Energy Used for Photoionization of the Subliming Products

	Ice Composition	Ratio	Thickness (nm)	Current (nA)	Irradiation Time (s)	Dose (eV CO molec^{-1})	Dose (eV H_2O molec^{-1})	photon energy (eV)
1	CO: H_2O	1.3 ± 0.5 : 1	1030 ± 50	50 ± 5	3600 ± 10	8 ± 2	5 ± 1	10.82
2	CO: H_2O	1.5 ± 0.5 : 1	900 ± 100	100 ± 5	2700 ± 10	12 ± 3	8 ± 2	10.49
3	CO: H_2O	1.0 ± 0.4 : 1	1000 ± 400	50 ± 5	7200 ± 10	15 ± 3	10 ± 2	10.23
4	CO: H_2O	1.0 ± 0.4 : 1	1000 ± 400	50 ± 5	3600 ± 10	8 ± 2	5 ± 1	9.75
5	CO: H_2O	1.0 ± 0.4 : 1	1000 ± 400	50 ± 5	3600 ± 10	15 ± 3	10 ± 2	9.10
6	CO: D_2O	1.0 ± 0.4 : 1	1280 ± 50	50 ± 5	7200 ± 10	15 ± 3	10 ± 2	10.82
7	CO: D_2O	0.6 ± 0.2 : 1	800 ± 200	100 ± 5	2700 ± 10	9 ± 3	6 ± 2	10.49
8	CO: D_2O	0.7 ± 0.2 : 1	1100 ± 100	50 ± 5	7200 ± 10	13 ± 3	9 ± 2	10.23
9	^{13}CO: H_2O	1.9 ± 0.5 : 1	1200 ± 500	50 ± 5	7200 ± 10	17 ± 3	12 ± 2	10.82
10	^{13}CO: D_2O	0.8 ± 0.3 : 1	1650 ± 500	50 ± 5	7200 ± 10	14 ± 3	9 ± 2	10.82
11	$C^{18}O$: $H_2^{18}O$	1.0 ± 0.4 : 1	1000 ± 200	50 ± 5	3600 ± 10	8 ± 2	5 ± 1	10.82

Table 2
Parameters for the Vacuum Ultraviolet Light Generation Used in the Present Experiments

ω_1 (nm)	ω_2 (nm)	Nonlinear Medium	Four-wave Mixing Scheme[a]	ω_{VUV} (nm)	ω_{VUV} (eV)
202	859	Krypton	$2\omega_1 - \omega_2 = \omega_{VUV}$	115	10.82
355		Xenon	$3\omega_1 = \omega_{VUV}$	118	10.49
202	612	Krypton	$2\omega_1 - \omega_2 = \omega_{VUV}$	121	10.23
202	495	Krypton	$2\omega_1 - \omega_2 = \omega_{VUV}$	127	9.75
222	607	Xenon	$2\omega_1 - \omega_2 = \omega_{VUV}$	136	9.10

Note.
[a] Frequencies are used for four-wave mixing equations.

Kostko et al. 2008; Xu et al. 2019). Thus, the detection of formaldehyde at 10.82 eV is reasonable. The experiments using CO: D_2O(D_2CO, $m/z = 32$), ^{13}CO: H_2O($H_2^{13}CO$, $m/z = 31$), ^{13}CO: D_2O ($D_2^{13}CO$, $m/z = 33$), and $^{13}C^{18}O$: $H_2^{18}O$ ($H_2^{13}C^{18}O$, $m/z = 33$) revealed consistent results with the initial peak and similar results with the second peak, although sublimation temperatures, peak profiles, and peak intensities varied across experiments for the second peak.

CH_3OH

The signal at $m/z = 32$ belongs to the simplest alcohol, methanol (CH_3OH, Figure 3, center), which has an evaluated ionization energy of 10.84 ± 0.01 eV. Similar to the effects that reduce formaldehyde's ionization energy mentioned previously, methanol was seen at 10.82 eV photon energy, and this constituted the only prominent signal. The most intense and well-defined signal peaks at 174 K, which sublimes along with the water matrix, but at a higher temperature than formaldehyde, indicating that methanol is more closely bound to the water matrix. The signal continues to a series of broad, low-intensity peaks with prominences at approximately 196 and 224 K. Isotopically labeled ices present matching results and $m/z = 36$ (CO: D_2O, CD_3OD), $m/z = 33$ (^{13}CO: H_2O, $^{13}CH_3OH$), $m/z = 37$ ($^{13}CD_3OD$), and $m/z = 35$ ($^{13}C^{18}O$: $H_2^{18}O$, $^{13}CH_3^{18}OH$).

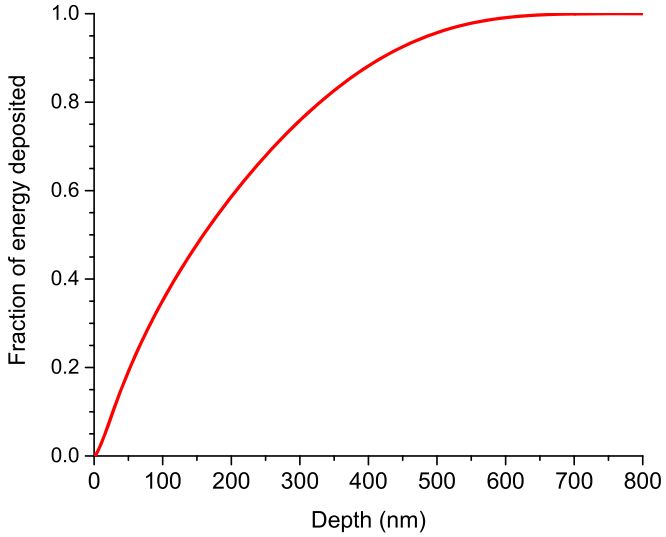

Figure 1. Fraction of 5 keV electron energy deposited as a function of depth as determined by CASINO calculations for Ice 1.

H_2O_2

The only compound without carbon detected using the PI-ReTOF-MS method was hydrogen peroxide at $m/z = 34$ (Figure 3, right). The evaluated ionization energy of 10.58 ± 0.04 eV is lower than formaldehyde and methanol, yet high enough that the primary signal occurred at 10.82 eV with only trace amounts seen at 10.49 eV. The initial signal peaks at 180 K and represents the completion of the water matrix sublimation to which hydrogen peroxide is tightly bound. A shoulder appears near 190 K followed by a resolved peak at 222 K. Compared to the formaldehyde and methanol profiles, hydrogen peroxide displays more variance between the sublimation profiles of the isotopically labeled ices. The CO: D_2O profile (D_2O_2) is obscured by the much more intense methanol (CD_3OD) signal at $m/z = 36$. The 222 K peak is

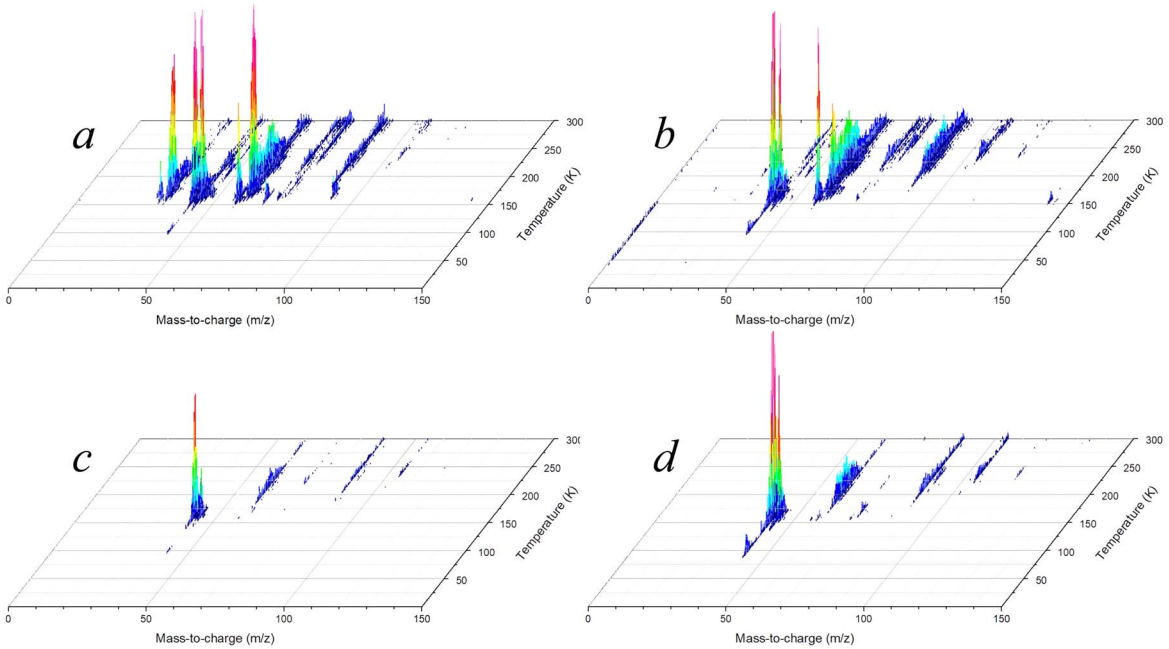

Figure 2. Temperature-dependent mass spectra of irradiated CO: H_2O ices as a function of temperature during TPD at photon energies of (a) 10.82 eV, (b) 10.49 eV, (c) 10.23 eV, and (d) 9.75 eV.

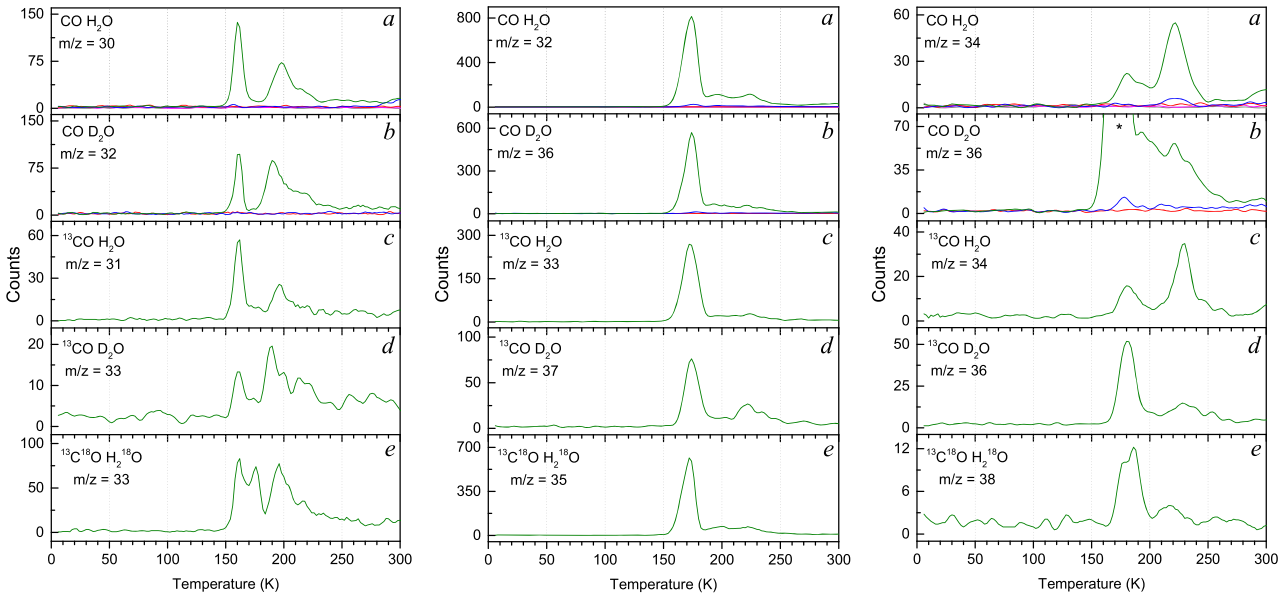

Figure 3. Sublimation profiles of H_2CO (left), CH_3OH (center), and H_2O_2 (right) observed at the indicated mass-to-charge ratios (m/z) corresponding to the isotopic labeling of the reactants. The profiles display traces at photon energies of 10.82 eV (green), 10.49 eV (blue), 10.23 eV (red), 9.75 eV (pink), and 9.10 eV (gray). *Right(b): Signal due to CD_3OD.

much weaker in the ^{13}CO: D_2O (D_2O_2, $m/z = 36$) and $^{13}C^{18}O$: $H_2^{18}O$ ($D_2^{18}O_2$, $m/z = 38$) ices, although the latter also has a much weaker intensity for all peaks. While only the ^{13}CO: H_2O profile (H_2O_2, $m/z = 34$) closely matches the non-isotopically labeled Ice 1, the formula H_2O_2 can still be assigned due to its ionization energy, the similarity of the sublimation profiles, and uniqueness of the mass-to-charge ratio 34.

C_2H_2O

These results, which predominantly belong to ketene (H_2CCO) with a minor amount of ethynol (HCCOH; Figure 4, left), are covered in detail by Turner et al. (2020).

C_2H_4O

Mass-to-charge 44 provides the first opportunity to exploit ionization energies to discriminate between isomers as well as multiple molecular formulas having $m/z = 44$. Given the CO: H_2O reactants, $m/z = 44$ could belong to the formulas for propane (C_3H_8), carbon dioxide (CO_2), and C_2H_4O, which has three isomers. Carbon dioxide can be eliminated from consideration as its evaluated ionization energy (13.777 ± 0.001 eV) is much higher than the highest photon energy used here (10.82 eV). Similarly, propane has a high ionization energy (10.94 ± 0.05 eV) that typically would not be seen at 10.82 eV, especially since, unlike formaldehyde (H_2CO) and methanol (CH_3OH), propane is not expected to sublime with the water matrix and have a lowered

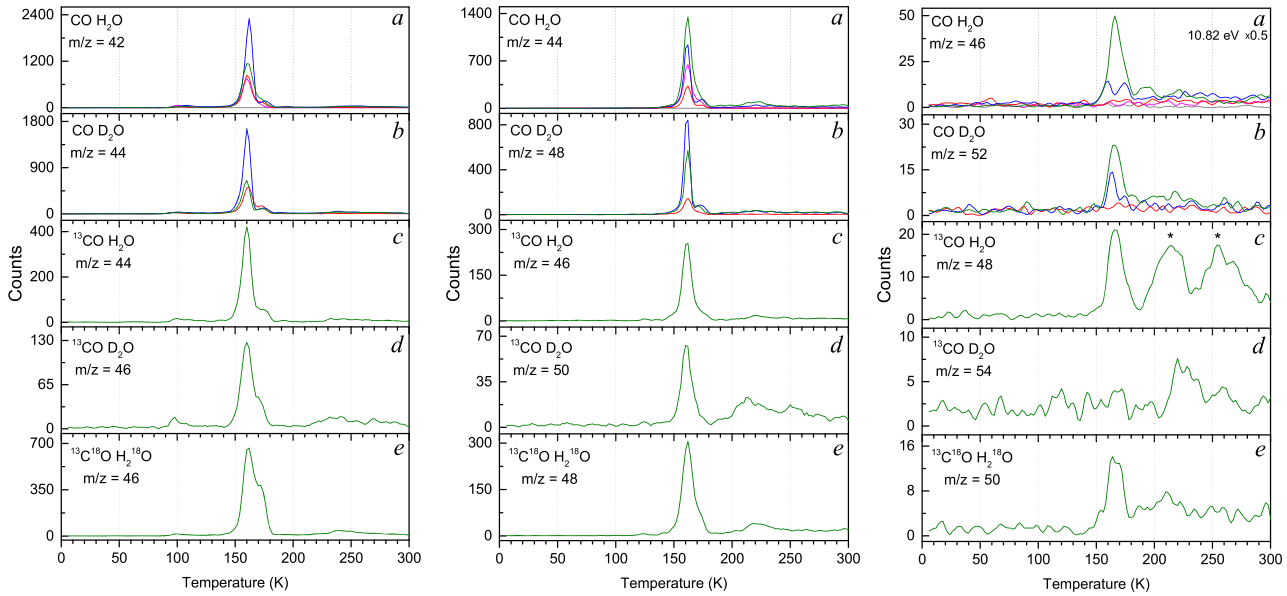

Figure 4. Sublimation profiles of C_2H_2O (left), C_2H_4O (center), and C_2H_6O (right) observed at the indicated mass-to-charge ratios (m/z) corresponding to the isotopic labeling of the reactants. The profiles display traces at photon energies of 10.82 eV (green), 10.49 eV (blue), 10.23 eV (red), 9.75 eV (pink), and 9.10 eV (gray). *Right(c): $^{13}CH_3O_2^+$.

ionization energy. The formula C_2H_4O belongs to three isomers: vinyl alcohol (CH_2CHOH, ionization energy (IE) = 9.17 ± 0.05 eV), acetaldehyde (CH_3CHO, IE = 10.229 ± 0.0007 eV), and ethylene oxide (c − C_2H_4O, IE = 10.56 ± 0.01 eV), and these ionization energies are needed to discriminate the isomers (Figure 4, center). The signals for C_2H_4O show a strong peak at 162 K proceeded by a shoulder that returns to baseline at 180 K, after which a broad low-intensity signal occurs between 200 and 240 K. These profiles are consistent in each isotopically labeled ice. The first peak and shoulder are observed at 10.82, 10.49, 10.23, and 9.75 eV, but not at 9.10 eV. This confirms the detection of vinyl alcohol (IE = 9.17 ± 0.05). The broad higher-temperature signals are seen at 10.82 and 10.49 eV, but at no lower photon energies. This suggests the presence of acetaldehyde (IE = 10.229 ± 0.0007), which would have a minimal signal at 10.23 eV and lower photon energies. These results are consistent with Abplanalp et al. (2016), who found that in irradiated CO:CH_4 ices the C_2H_4O signal was dominated by vinyl alcohol with a minor amount of acetaldehyde at higher temperatures. Given the data, the presence of ethylene oxide can neither be confirmed nor rejected.

C_2H_6O

Two molecular formulas can contribute to $m/z = 46$: CH_2O_2 (formic acid) and C_2H_6O (ethanol and dimethyl ether). Formic acid has an evaluated ionization energy of 11.33 ± 0.01 eV, which is above the highest photon energy of 10.82 eV. In addition, no signal is seen at $m/z = 51$ for $^{13}CH_2^{18}O_2$ in the $^{13}C^{18}O$: $H_2^{18}O$ ice, which verifies that formic acid does not contribute to the observed signals. Although the ionization threshold is too high to detect formic acid, it was previously detected spectroscopically in irradiated CO: H_2O ice mixtures (Bennett et al. 2011). Thus, the data is assigned to C_2H_6O, which has evaluated ionization energies of 10.48 ± 0.07 eV for ethanol (CH_3CH_2OH) and 10.025 ± 0.025 eV for dimethyl ether (CH_3OCH_3; Figure 4, right). At 10.82 eV, a strong peak occurs at 166 K with a shoulder at 174 K. However, at 10.49 eV, this temperature range is composed of two separated peaks at 160 and 174 K. These two peaks at 10.49 eV are observed in both the CO: H_2O and CO: D_2O ices, while the single peak with shoulder at 10.82 eV is seen in the CO: H_2O, CO: D_2O, ^{13}CO: H_2O, and $^{13}C^{18}O$: $H_2^{18}O$ ices. The peak shape for the ^{13}CO: D_2O ice cannot be described due to the weaker signal for the ^{13}CO: D_2O ice mixture. The lack of signal at 10.23 eV, however, eliminates dimethyl ether from consideration (IE = 10.025 ± 0.025 eV) and indicates these data result from ethanol (IE = 10.48 ± 0.07 eV). The evaluated ionization is near the experimental 10.49 eV photon energy used but has a relatively large error range (±0.07 eV), and so an observed signal at 10.82 eV and 10.49 eV is consistent with ethanol. In addition, the variation in sublimation profiles can be understood as differences in sublimation environments within the water matrix, because as previously discussed, co-sublimation with water can affect the ionization energy of compounds. In addition, previous results of irradiated CH_4: H_2O ices (Bergantini et al. 2017) also found evidence of ethanol subliming with the water matrix and did not observe dimethyl ether, which was confirmed by doping the CH_4: H_2O ices to 1% dimethyl ether and observing that dimethyl ether sublimes before the water matrix with peaks at 115 and 135 K. These lower-temperature peaks are also not observed in the present CO: H_2O ices.

$C_2H_2O_2$

For $m/z = 58$, three molecular formulas are viable: $C_2H_2O_2$, C_3H_6O, and C_4H_{10}. Based on isotopically labeled experiments, only $C_2H_2O_2$ could be assigned and confirmed (Figure 5, left). Three isomers were investigated for $C_2H_2O_2$: glyoxal (CHO-CHO), hydroxyketene (HOCHCO), and ethynediol (HOCCOH). Unlike previously discussed products, the isomers of $C_2H_2O_2$ have limited experimentally determined ionization energies, and only glyoxal has been evaluated (10.2 eV). Calculated adiabatic ionization energies for hydroxyketene (8.44 eV) and ethynediol (8.66 eV) were determined (Vijay & Sastry 2005), both of which are below the lowest experimental photon energy of 9.10 eV. By comparison, the same study calculated the ionization energy of glyoxal to be 9.87–9.97 (for the trans-cis conformers), which is approximately 0.2–0.3 eV lower than the evaluated ionization energy. The TPD profiles show a strong peak at 160 K followed

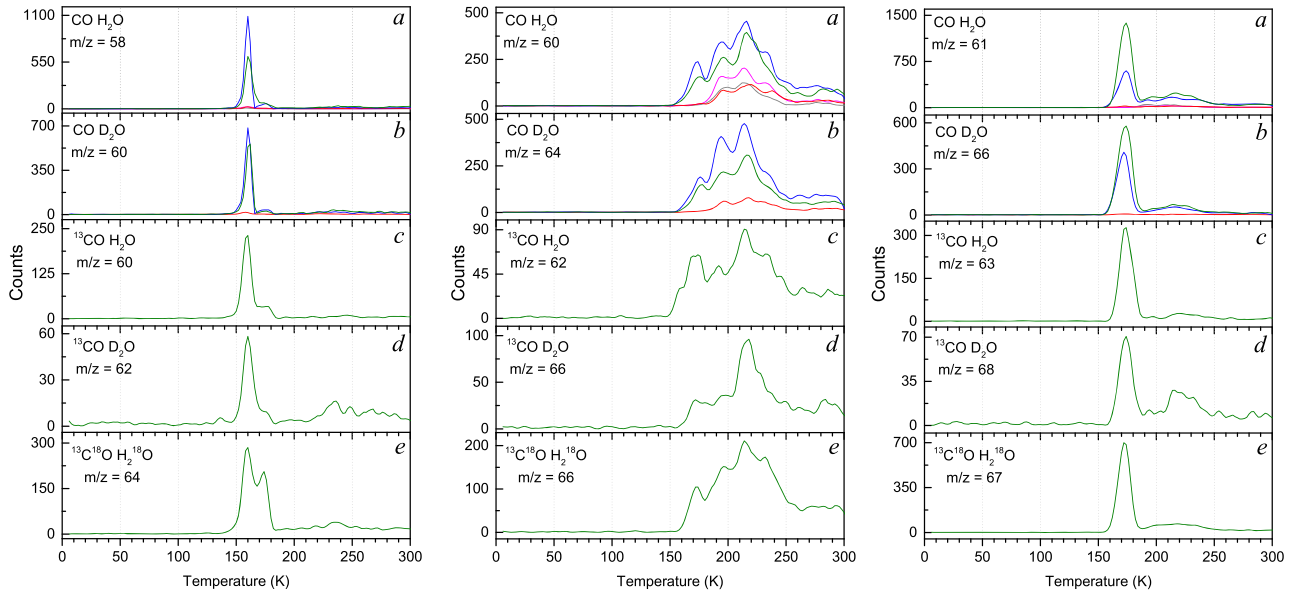

Figure 5. Sublimation profiles of $C_2H_2O_2$ (left), $C_2H_4O_2$ (center), and $C_2H_5O_2^+$ (right) observed at the indicated mass-to-charge ratios (m/z) corresponding to the isotopic labeling of the reactants. The profiles display traces at photon energies of 10.82 eV (green), 10.49 eV (blue), 10.23 eV (red), 9.75 eV (pink), and 9.10 eV (gray).

by a less intense peak at 176 K in the 10.82 and 10.49 eV profiles. This profile matches those in the isotopically labeled profiles, although the 176 K peak is more intense in the $^{13}C^{18}O$: $H_2^{18}O$ ice. At 10.23 eV and lower photon energies, only a negligible peak is observed. Thus, glyoxal (CHOCHO) is the only significant contributor to these signals.

$C_2H_4O_2$

The investigation into the source of $m/z = 60$ found that isotopically labeled experiments were consistent with $C_2H_4O_2$, but not C_3H_8O. Five isomers of $C_2H_4O_2$ are considered, two of which have evaluated experimental ionization energies (IE_{eval}), while the ionization energies of all five isomers were calculated (IE_{calc}) by Kleimeier et al. (2020a). With increasing ionization energy, these include 1,2-ethenediol (HOCHCHOH, IE_{calc} = 8.16–8.37 eV), 1,1-ethenediol ($CH_2C(OH)_2$, IE_{calc} = 8.59–8.68 eV), glycolaldehyde ($HOCH_2CHO$, IE_{calc} = 9.84–10.06 eV), acetic acid (CH_3COOH, IE_{eval} = 10.65 eV, IE_{calc} = 10.52–10.65 eV), and methyl formate (CH_3OCHO, IE_{eval} = 10.835 eV, IE_{cal} = 10.68–10.83 eV) with ranges of calculated ionization energies presented for the various calculated conformers (Figure 5, center). Unlike the profiles of lower-mass products, which were dominated by a distinct peak co-subliming with water, the profiles for $C_2H_4O_2$ show numerous peaks beginning at 150 K and remaining to 300 K. Notable peaks include 174 K, which is present only at 10.82 and 10.49 eV but not at lower photon energies, as well as 194, 214, and 232 K, which are present at all photon energies. Methyl formate (IE_{eval} = 10.835 eV) cannot be assigned because its ionization is slightly above the highest photon energy (10.82 eV), and no peak is seen at 10.82 eV that is absent at 10.49 eV. The signals at 9.10 eV indicate the presence of 1,2-ethenediol and/or 1,1-ethenediol, which both have ionization energies below 9.10 eV, but these data prevent further discrimination. Given the ionization energy range of glycolaldehyde (9.84–10.06 eV), an assignment could be made if a peak were observed at 10.23 eV, but not 9.75 eV; however, no such peak exists, and thus glycolaldehyde cannot be assigned. The remaining isomer, acetic acid, is best assigned to the peak at 174 K. Although the ionization energies are higher than 10.49 eV, the lowest calculated ionization energy is only slightly higher at 10.52 eV; sublimation at 174 K indicates co-sublimation with water, which, as with several lower-mass products, can lower the effective ionization energy. Additional support for the assignment of acetic acid to the 174 K can be found in the next section, $C_2H_5O_2^+$.

$C_2H_5O_2^+$

The protonated monomer $C_2H_5O_2^+$ ($m/z = 61$) is notable, as previous studies of irradiated ices (Bergantini et al. 2018c; Kleimeier et al. 2020a) have found that acetic acid (CH_3COOH) presents predominantly as $C_2H_5O_2^+$ in PI-ReTOF-MS studies rather than the unprotonated molecular ion ($m/z = 60$); it has been observed as a dissociation product of photoionized acetic acid dimers (Guan et al. 2012). A single intense peak is observed at 174 K—the same temperature assigned to acetic acid in the previous discussion—at 10.82 and 10.49 eV but not at lower photon energies, and this peak is at the same temperature for all isotopic labeling (Figure 5, right). Thus, this peak is assigned to $C_2H_5O_2^+$ and is considered a proxy for the detection of acetic acid, which was also observed as a monomer at $m/z = 60$.

$C_2H_6O_2$

Isotopically labeled experiments for the CO: H_2O peak at $m/z = 62$ revealed the formula $C_2H_6O_2$ (Figure 6, left). Four isomers of $C_2H_6O_2$ are considered although $m/z = 62$ marks a transition from smaller-mass products in which the ionization energies for the various isomers of higher-mass products become scarcer. No ionization energy, experimental nor calculated, was found for 1,1-ethanediol ($CH_3CH(OH)_2$), and thus this isomer cannot be assigned. The ionization of dimethyl peroxide (CH_3OOCH_3) was found to be 9.1 eV using photoelectron spectroscopy (Kimura & Osafune 1975); although only vertical, and not adiabatic, ionization energies using photoelectron spectroscopy were found for ethylene glycol (1,2-ethanediol, $HOCH_2CH_2OH$, $IE_{vertical}$ = 10.55 eV). No experimental value was found for methoxymethanol (CH_3OCH_2OH). However, Zhu et al. (2019) calculated the ionization energies for dimethyl peroxide (9.31 eV), ethylene glycol (9.76–9.79 eV), and methoxymethanol (10.01–10.29 eV). The TPD profiles show two primary sublimation regions peaking at

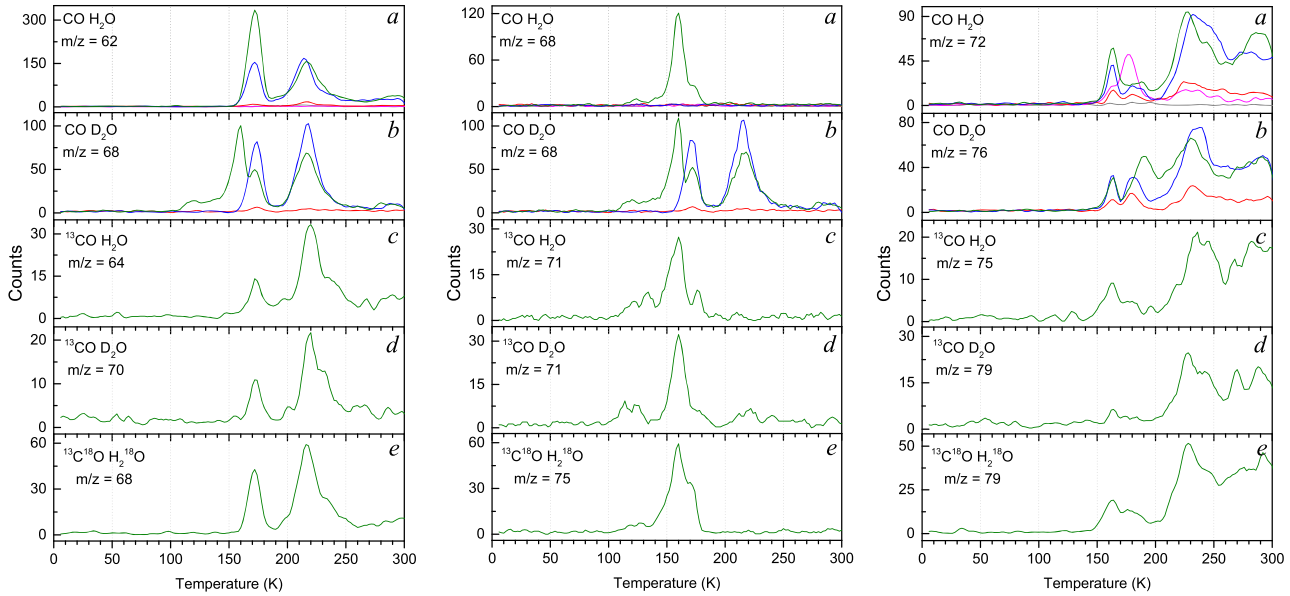

Figure 6. Sublimation profiles of $C_2H_6O_2$ (left), C_3O_2 (center), and $C_3H_4O_2$ (right) observed at the indicated mass-to-charge ratios (m/z) corresponding to the isotopic labeling of the reactants. The profiles display traces at photon energies of 10.82 eV (green), 10.49 eV (blue), 10.23 eV (red), 9.75 eV (pink), and 9.10 eV (gray). Note that $m/z = 68$ is shown for both CO: D_2O profiles (b) for left and center and that this profile contains signals for both $C_2D_6O_2$ and C_3O_2.

172 and 216 K with a higher-temperature shoulder at 234 K. Strong signals are observed for both sublimation regions at 10.82 and 10.49 eV with a minor signal at 10.23 eV and no signal at 9.75 and 9.10 eV. The absence of a signal at 9.75 eV eliminates dimethyl peroxide while the stronger signal at 10.82 and 10.49 eV indicates the presence of methoxymethanol, which has a calculated ionization energy of 10.29 eV for its most stable conformer. The remaining signal at 10.23 eV could be due to other conformers of methoxymethanol or to ethylene glycol. Previous studies of irradiated methanol-d_3 (CD_3OH) ice found that methoxymethanol has two sublimation regions (168 and 200 K), similar to the present CO: H_2O ices, and unlike ethylene glycol with only one sublimation peak (200 K; Zhu et al. 2019). Thus, the current data confirms the presence of methoxymethanol; ethylene glycol cannot be positively assigned.

C_3O_2

While C_4H_4O was investigated for $m/z = 68$, this mass unambiguously belongs to C_3O_2 (1,3-propadiene-1,3-dione, OCCCO) with an experimental ionization energy of 10.60 eV (Baker & Turner 1968). Three peaks are seen in the sublimation profiles only at 10.82 eV (Figure 6, center): a small peak at 124 K, an intense second peak at 160 K, and a less intense third peak at 174 K. Given that the signal is only seen at 10.82 eV and not 10.49 eV or lower photon energies, as well as the matching isotopically labeled profiles, C_3O_2 is assigned to $m/z = 68$.

$C_3H_4O_2$

Mass-to-charge ratio 72 was found to belong to the molecular formula $C_3H_4O_2$ based on the isotopically labeled experiments (Figure 6, right), but the large number of possible isomers, lack of most ionization energies, and complex TPD profiles limit the ability to fully assign the peaks. The evaluated ionization energy is provided for just one isomer (2-propenoic acid, $CH_2CHCOOH$, IE = 10.60 eV). The TPD profiles contain two small peaks at 164 and 180 K, followed by a more intense peak at 230 K. Several poorly defined peaks persist to 300 K. The sublimation profile shapes are approximately consistent between 10.82, 10.49, 10.23, and 9.75 eV except that, in general, intensity declines with decreasing photon energy. The signal is negligible at 9.10 eV. In the absence of a peak that is present at 10.82 eV but absent at all lower photon energies, 2-propenoic acid cannot be assigned. Given the available ionization energies and TPD profiles, no isomers can be assigned.

$C_2H_2O_3$

The formula $C_2H_2O_3$ was assigned to $m/z = 74$ as well as the corresponding masses in each of the isotopically labeled experiments (Figure 7, left). This formula includes two isomers of note: glyoxylic acid (HCOCOOH) and formic anhydride (HCOOCHO). These results have been reported previously with the identification of glyoxylic acid (Eckhardt et al. 2019).

$C_2H_4O_3$

Mass-to-charge ratio 76 belongs to $C_2H_4O_3$, and the sublimation profiles for CO: D_2O ($C_2D_4O_3$, $m/z = 80$), ^{13}CO: H_2O ($^{13}C_2H_4O_3$, $m/z = 78$), ^{13}CO: D_2O ($^{13}C_2D_4O_3$, $m/z = 82$), and $^{13}C^{18}O$: $H_2^{18}O$ ($^{13}C_2H_4^{18}O_3$, $m/z = 84$) match well (Figure 7, center). An initial signal is seen at 168 K but remains low until the first prominent peak at 232 K. This is followed by a more intense peak at 258 K, and finally 296 K. Several small peaks and shoulders exist, notably a shoulder before the first peak, another shoulder after the second peak, and a small peak at 286 K. The TPD profiles at 10.82 and 10.49 eV photon energy are similar, while at 10.23 eV, the signal is weaker but several peaks are discernible, including 232, 254, and 294 K. These correlate with the three prominent peaks mentioned at 10.82 eV. Only a trace signal persists at 9.75 and 9.10 eV. Several isomers are possible, including glycolic acid ($HOCH_2COOH$), but without a set of known ionization energies, further identification of the isomers is not possible.

$C_3H_4O_3$

The formula $C_3H_4O_3$ is assigned to $m/z = 88$, and similar sublimation profiles are seen with isotopic labeling (Figure 7, right). The first sublimation peaks at 193 K, and the signal rises to two similar intensity peaks at 216 and 242 K. The signal intensities decline with decreasing photon energy until only a trace signal remains at 9.10 eV, but each of the peaks are seen from 9.75 to 10.82 eV. The $C_3H_4O_3$ is associated with many

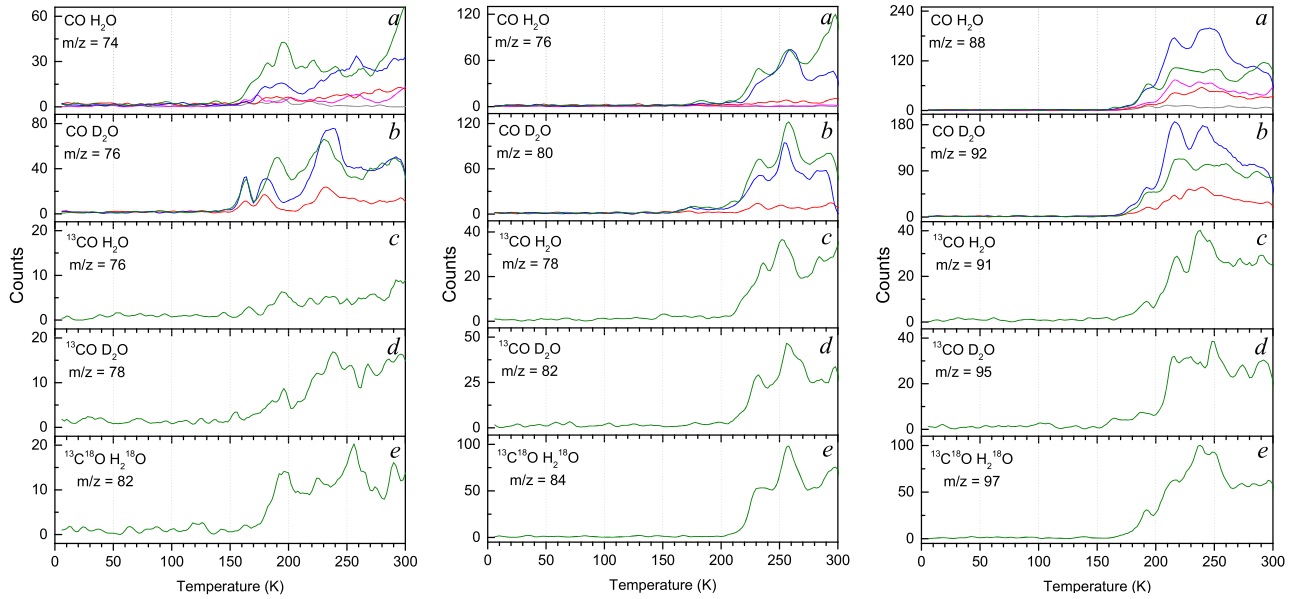

Figure 7. Sublimation profiles of $C_2H_2O_3$ (left), $C_2H_4O_3$ (center), and $C_3H_4O_3$ (right) observed at the indicated mass-to-charge ratios (m/z) corresponding to the isotopic labeling of the reactants. The profiles display traces at photon energies of 10.82 eV (green), 10.49 eV (blue), 10.23 eV (red), 9.75 eV (pink), and 9.10 eV (gray).

isomers, including pyruvic acid ($CH_3COCOOH$, IE = 9.90 eV), which has been previously discovered in irradiated laboratory ices of acetaldehyde and carbon dioxide (Kleimeier et al. 2020b). However, given the current sublimation profiles and numerous isomers without known ionization energies, no definitive isomer assignments can be determined.

$C_3H_6O_3$

Two formulas were closely investigated for $m/z = 90$: $C_3H_6O_3$ and $C_2H_2O_4$ (such as oxalic acid). While deuterium substitution ($C_2D_2O_4$, $m/z = 92$ and $^{13}C_2D_2O_4$, $m/z = 94$) generally supported the $C_2H_2O_4$ assignment, the profiles for $^{13}C_2H_2O_4$ ($m/z = 92$) and $^{13}C_2H_2^{18}O_4$ ($m/z = 100$) did not contain similar peaks, and thus only $C_3H_6O_3$ is considered (Figure 8, left). The initial sublimation event peaks at 217 K and is followed by a more intense peak at 240 K. After a shoulder at 254 K, the signal remains elevated, but distinct peaks are absent. Similar sublimation profiles are seen in the isotopically labeled experiments except for ^{13}CO: D_2O ($^{13}C_3D_6O_3$, $m/z = 99$), which has poorly resolved peaks due to the low signal intensity characteristic of this ice mixture. Also, the ^{13}CO: H_2O profile ($m/z = 93$) displayed a peak at 170 K belonging to $^{13}C_2H_3O_4^+$. The first two peaks are observed at all photon energies, while the signals at higher temperatures are diminished below the 10.82 and 10.49 eV photon energies. While individual isomers cannot be identified, notable isomers of $C_3H_6O_3$ include lactic acid ($CH_3CHOHCOOH$), glyceraldehyde ($HOCH_2CHOHCHO$), and dihydroxyacetone ($HOCH_2COCH_2OH$).

$C_3H_4O_4$

The sublimation profile for $m/z = 104$ belongs to $C_3H_4O_4$ (Figure 8, center). The primary, intense peak for each isotopically labeled system occurs at 242 K, while a second peak or shoulder appears around 264 K. Similar profiles are observed at each photon energy. Although no adiabatic ionization energies for this formula are available from NIST, one notable isomer is malonic acid ($HOOCCH_2COOH$).

$C_4H_6O_4$

The highest mass observed was $m/z = 118$ and is assigned to $C_4H_6O_4$ (Figure 8, right). The profiles are similar to those for $C_3H_4O_4$, albeit only about a third as intense. The first, strongest peak occurs at 246 K and is followed by a less intense peak or shoulder around 258 K. Other than relative intensity, minimal differences are seen between photon energies. The profiles are most intense in the CO: H_2O and CO: D_2O ices while a low signal in the ^{13}CO: H_2O and ^{13}CO: D_2O ices results in poorly resolved peaks. It is notable that the highest masses observed ($m/z = 90$, 104, and 118) are separated by 14 mass units, although the atomic explanations are distinct. Between $m/z = 90$ and 104, the formula includes an additional oxygen atom with two fewer hydrogen atoms, which results in a difference of 14 mass units. However, from $m/z = 104$ to 118, the formula adds an additional carbon atom and two hydrogen atoms. Thus, the formulas for $m/z = 90$ and 118 differ by one carbon monoxide (CO) unit. Like other high mass profiles, individual isomers cannot be identified, but a representative isomer of $C_4H_6O_4$ is succinic acid ($HOOCCH_2CH_2COOH$), which, like malonic acid ($C_3H_4O_4$, $m/z = 104$), is a dicarboxylic acid. However, succinic acid has an additional CH_2 moiety connecting the carboxylic acid groups.

4. Discussion

The aforementioned results demonstrate that complex organic molecules as large as $C_4H_6O_4$ can be formed under astrophysical conditions from ices of carbon monoxide and water, which shows an important link between inorganic starting materials and complex organic products. Figure 9 displays extracted formation pathways toward each of the isomers identified from Figures 3–8 and illustrates the processes by which complex organic molecules can form on interstellar icy grains. Initial reactions of the reactants break down water to the hydroxyl radical and atomic hydrogen (reaction 1; Zheng et al. 2006a, 2006b, 2007), while the reaction of two carbon monoxide molecules produces dicarbon monoxide and atomic oxygen (reaction 2; Jamieson et al. 2006; Maity et al. 2014;

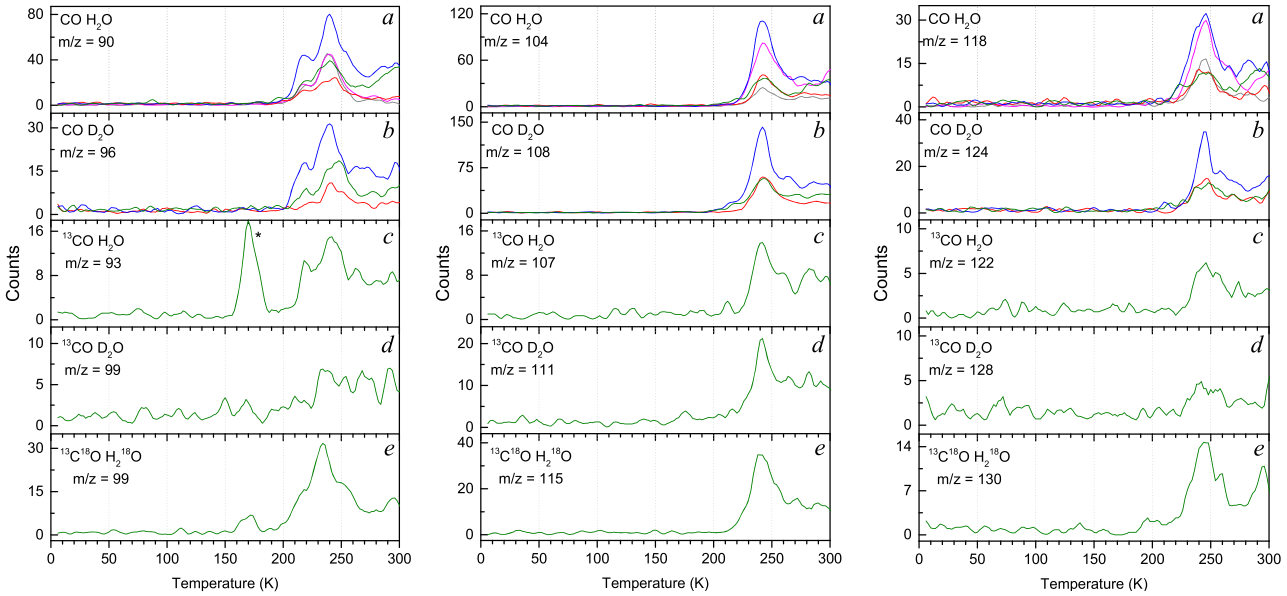

Figure 8. Sublimation profiles of $C_3H_6O_3$ (left), $C_3H_4O_4$ (center), and $C_4H_6O_4$ (right) observed at the indicated mass-to-charge ratios (m/z) corresponding to the isotopic labeling of the reactants. The profiles display traces at photon energies of 10.82 eV (green), 10.49 eV (blue), 10.23 eV (red), 9.75 eV (pink), and 9.10 eV (gray). *Left(c): $^{13}C_2H_3O_4^+$.

Turner et al. 2020).

$$H_2O \rightarrow OH(X^2\Pi) + H(^2S)\Delta G_r = 545 \text{ kJ mol}^{-1} \quad (1)$$

$$2CO \rightarrow CCO(X^3\Pi) + O(^3P)\Delta G_r = 852 \text{ kJ mol}^{-1}. \quad (2)$$

As these reactions are strongly endoergic, an external source of energy is necessary to initiate these nonequilibrium reactions in cold interstellar ices. The two inorganic products, hydrogen peroxide and carbon suboxide, are products of pure reactant ices (Zheng et al. 2006a; Bennett et al. 2008), and they proceed, respectively, via radical–radical recombination of hydroxyl radicals (reaction 3) and the reaction of dicarbon monoxide radical with carbon monoxide (reaction 4).

$$2OH(X^2\Pi) \rightarrow H_2O_2 \quad (3)$$

$$CCO(X^3\Pi) + CO \rightarrow C_3O_2. \quad (4)$$

Several organic molecules form through successive hydrogenation of precursors, the simplest example being the hydrogenation of carbon monoxide to formaldehyde via the formyl radical (reactions 5, 6; Bennett et al. 2011; Eckhardt et al. 2019).

$$CO + H(^2S) \rightarrow HCO(X^2A') \quad (5)$$

$$HCO(X^2A') + H(^2S) \rightarrow H_2CO. \quad (6)$$

The hydrogenation of formaldehyde leads to methanol (reaction 7; Bennett et al. 2007).

$$H_2CO + 2H(^2S) \rightarrow CH_2OH/CH_3O + H \rightarrow CH_3OH. \quad (7)$$

Further reaction of two methanol molecules can lead to methoxymethanol (reaction 8) via recombination of the methoxy radical and the hydroxymethylene radical (Zhu et al. 2019).

$$CH_2OH + CH_3O \rightarrow CH_3OCH_2OH. \quad (8)$$

Two formyl radicals can undergo radical–radical recombination leading to glyoxal (reaction 9; Abplanalp & Kaiser 2019).

$$2HCO(X^2A') \rightarrow CHOCHO. \quad (9)$$

Glyoxal can then be hydrogenated to produce ethenediol (reaction 10). These experiments were unable to discriminate between the isomers of ethenediol: 1,1-ethenediol and cis/trans 1,2-ethenediol. However, as 1,1-ethenediol was only recently discovered (Mardyukov et al. 2020), the more stable 1,2-ethenediol is used to represent these isomers.

$$CHOCHO + 2H(^2S) \rightarrow HOCHCHOH. \quad (10)$$

The reaction of the hydroxyl radical with carbon monoxide leads to the hydroxycarbonyl radical (HOCO, reaction 11; Bennett et al. 2011; Eckhardt et al. 2019).

$$CO + OH(X^2\Pi) \rightarrow HOCO(X^2A'). \quad (11)$$

The HOCO radical serves as an intermediate in the formation pathways of diverse carboxylic acids including benzoic acid (McMurtry et al. 2016a), nicotinic acid (niacin; McMurtry et al. 2016b), 2-sila acetic acid (Chandra et al. 2021), and phosphino formic acid (Zhu et al. 2018). The reaction of HOCO with a hydrogen atom likely generates formic acid in the CO: H_2O ices, which also could be formed by radical–radical recombination of formyl and hydroxyl radicals (Bennett et al. 2011), but the high ionization energy of formic acid prevents detection in these experiments. However, recombination of HOCO with a formyl radical leads to glyoxylic acid (reaction 12; Eckhardt et al. 2019).

$$HOCO(X^2A') + HCO((X^2A') \rightarrow CHOCOOH. \quad (12)$$

The dicarbon monoxide radical can also undergo a series of hydrogenation steps beginning with the formation of the first keto-enol equilibrium pair: ketene and ethynol (reactions 13, 14; Turner et al. 2020).

$$CCO(X^3\Pi) + 2H(^2S) \rightarrow H_2CCO \quad (13)$$

$$CCO(X^3\Pi) + 2H(^2S) \rightarrow HCCOH. \quad (14)$$

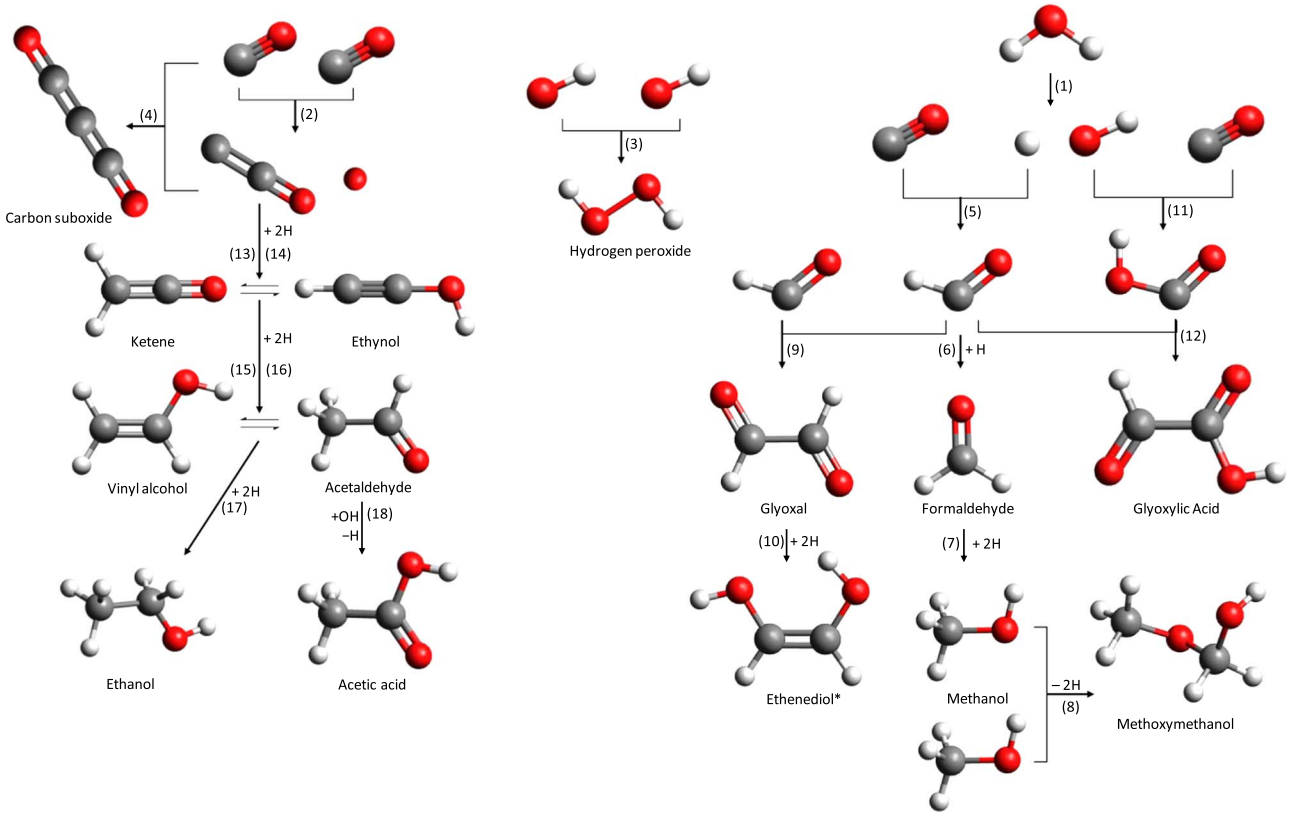

Figure 9. Reaction pathways from carbon monoxide and water leading to the products determined by PI-ReTOF-MS. Isomers confirmed in the experiments are labeled with names. Numbers in parentheses indicate confirmed reaction pathways described in Section 4. *The ethenediol isomers (1,1-ethenediol and cis/trans 1,2-ethenediol) could not be discriminated.

Hydrogenation of either of these C_2H_2O isomers leads to the second keto-enol equilibrium pair: vinyl alcohol and acetaldehyde (reactions 15, 16), which have also been detected in irradiated ices of carbon monoxide and methane (Abplanalp et al. 2016).

$$C_2H_2O + 2H(^2S) \rightarrow CH_2CHOH \quad (15)$$

$$C_2H_2O + 2H(^2S) \rightarrow CH_3CHO. \quad (16)$$

Further hydrogenation of these C_2H_4O isomers leads to saturated ethanol (reaction 17). While ethanol is often reported in appropriate ices with *organic* carbon sources such as CH_4: H_2O ice (Bergantini et al. 2017) or methanol-containing ices (Bergantini et al. 2018b; Zhu et al. 2020), the production of ethanol in the present ices is notable due to the *inorganic* carbon source.

$$C_2H_4O + 2H(^2S) \rightarrow CH_3CH_2OH. \quad (17)$$

A reaction from acetaldehyde to acetic acid involves hydrogen-loss from acetaldehyde and subsequent radical–radical recombination with a hydroxyl radical (reaction 18; Kleimeier et al. 2020a).

$$CH_3CHO \rightarrow CH_3CO + H(^2S) \quad (18a)$$

$$CH_3CO + OH(X^2\Pi) \rightarrow CH_3COOH. \quad (18b)$$

These various pathways that include radical–radical recombination, hydrogenation, and addition of lone atoms demonstrate that complex organic molecules as large as acetic acid ($C_2H_4O_2$), ethenediol ($C_2H_4O_2$), and methoxymethanol ($C_2H_6O_2$) can form stepwise starting with simple inorganic precursors such as water and carbon monoxide. These stepwise reactions are expected to continue toward $C_3H_4O_4$ and $C_4H_6O_4$, which are the largest formulas confirmed in this study but with isomers that cannot be determined due to limited ionization energy data and increasingly complex TPD profiles.

5. Astrophysical Implications

These results provide critical evidence that COMs can form on interstellar icy grains by abundant inorganic precursor molecules (carbon monoxide and water) that can leave the ices, either through sublimation or ejection, and become incorporated into the gaseous ISM. Recent studies have demonstrated that COMs can form in low-temperature ices at 5 K during irradiation (Abplanalp et al. 2018; Turner et al. 2018; Kleimeier et al. 2021) and do not require the diffusion of heavier species through the ice at higher temperatures during the TPD phase (Garrod et al. 2008). Thus, these irradiated analog ices and formation mechanisms can simulate the chemistry of interstellar icy grains toward the production of complex organic molecules. Of the product isomers detected using PI-ReTOF-MS, only formaldehyde (H_2CO) and methanol (CH_3OH) are known to exist on interstellar icy grains (Boogert et al. 2015). In addition, the following product isomers have been detected in the gas phase of the interstellar or circumstellar medium: hydrogen peroxide (Bergman et al. 2011), ethanol (Zuckerman et al. 1975; Pearson et al. 1997), vinyl alcohol (Turner & Apponi 2001), methoxymethanol (McGuire et al. 2017), acetaldehyde (Gottlieb 1973; Fourikis et al. 1974; Gilmore et al. 1976), ketene (Turner 1977), and acetic acid

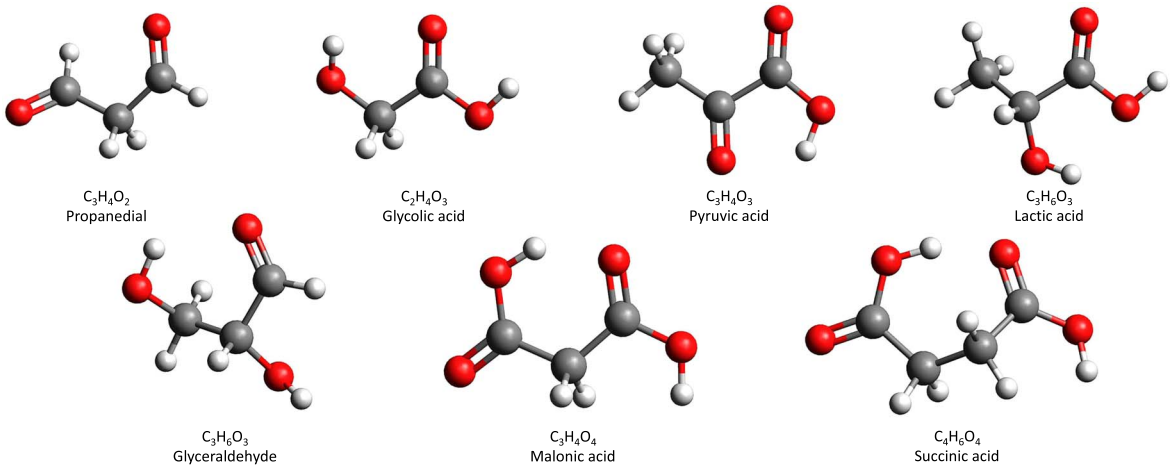

Figure 10. Chemical formulas confirmed by isotopic experiments, but for which isomeric distinctions could not be made. Representative isomers for each chemical formula are shown.

(Mehringer et al. 1997). Furthermore, carbon dioxide, a known component of interstellar ice (Boogert et al. 2015), and formic acid (Zuckerman et al. 1971; Winnewisser & Churchwell 1975) were detected spectroscopically in previous studies of this ice system (Bennett et al. 2011), but have ionization energies too high for the present PI-ReTOF-MS experiment. Of the higher-order formulas in which isomeric discrimination was not possible ($C_3H_4O_2$, $C_2H_4O_3$, $C_3H_4O_3$, $C_3H_6O_3$, $C_3H_4O_4$, $C_3H_6O_3$, and $C_4H_6O_4$), none have yet been discovered in the ISM (Woon 2021). Other compounds detected in this study that have yet to be discovered in the ISM include glyoxal, glyoxylic acid, ethynol, carbon suboxide, and the ethenediol isomers. Thus, the present work demonstrates that many known interstellar compounds can form in ices of carbon monoxide and water, and that several more can be expected. The results provide the astronomical observation community with potential targets to investigate. While the products are *complex* and *organic*, the starting material is *simple* and *inorganic*, which shows the interconnectivity between different classes of molecules and expands astrochemical knowledge as to possible formation pathways. After formation, these complex organic molecules could potentially find their way to planets such as the early Earth on comets or meteorites and provide chemical feedstock for the first life on Earth. Of the detected isomers, glyoxylic acid has perhaps the most notable astrobiological significance as it participates in the glyoxylate cycle (Kondrashov et al. 2006). This cycle also involves succinic acid ($C_4H_6O_4$), which has the highest-mass formula confirmed in this experiment. Each of the molecules in Figure 10, which were chosen to represent confirmed molecular formulas in which isomeric discrimination was not possible, have biological significance. Glycolic acid ($C_2H_4O_3$) is associated with photorespiration (South et al. 2017); propanedial (malondialdehyde, $C_3H_4O_2$) results from oxidation of polyunsaturated lipids (Davey et al. 2005); pyruvic acid ($C_3H_4O_3$), lactic acid ($C_3H_6O_3$), and glyceraldehyde ($C_3H_6O_3$) are involved in metabolism (Sillero et al. 1969; Summermatter et al. 2013; Kleimeier et al. 2020b), while malonic acid ($C_3H_4O_4$) derivatives were found as an intermediate in fatty acid synthesis (Wakil 1958). Given the number of biological functions for many of these products, the reaction of carbon monoxide and water on interstellar icy grains is of notable astrobiological importance. With further experiments and improved detection techniques, the astrobiological link between reactions on icy grains and early life on Earth will continue advancing and contributing to our knowledge of the origin of life.

This research was supported by the US National Science Foundation (NSF), Division for Astronomy (NSF-AST1800975). The W. M. Keck Foundation and the University of Hawaii at Manoa financed the construction of the experimental setup. N.F.K. acknowledges funding from the Deutsche Forschungsgemeinschaft (DFG, German Research Foundation) for a postdoctoral fellowship (KL 3342/1-1).

ORCID iDs

Alexandre Bergantini https://orcid.org/0000-0003-2279-166X
Cheng Zhu https://orcid.org/0000-0002-7256-672X
André K. Eckhardt https://orcid.org/0000-0003-1029-9272
Ralf I. Kaiser https://orcid.org/0000-0002-7233-7206

References

Abplanalp, M. J., Gozem, S., Krylov, A. I., et al. 2016, PNAS, 113, 7727
Abplanalp, M. J., Jones, B. M., & Kaiser, R. I. 2018, PCCP, 20, 5435
Abplanalp, M. J., & Kaiser, R. I. 2019, PCCP, 21, 16949
Al-Halabi, A., Fraser, H., Kroes, G., et al. 2004, A&A, 422, 777
Awad, Z., Chigai, T., Kimura, Y., et al. 2005, ApJ, 626, 262
Baker, C., & Turner, D. 1968, ChCom, 7, 400
Belau, L., Wilson, K. R., Leone, S. R., et al. 2007, JPCA, 111, 7562
Bennett, C. J., Chen, S. H., Sun, B. J., et al. 2007, ApJ, 660, 1588
Bennett, C. J., Hama, T., Kim, Y. S., et al. 2011, ApJ, 727, 27
Bennett, C. J., Jamieson, C. S., & Kaiser, R. I. 2008, P&SS, 56, 1181
Bergantini, A., Abplanalp, M. J., Pokhilko, P., et al. 2018a, ApJ, 860, 108
Bergantini, A., Góbi, S., Abplanalp, M. J., et al. 2018b, ApJ, 852, 70
Bergantini, A., Maksyutenko, P., & Kaiser, R. I. 2017, ApJ, 841, 96
Bergantini, A., Zhu, C., & Kaiser, R. I. 2018c, ApJ, 862, 140
Bergman, P., Parise, B., Liseau, R., et al. 2011, A&A, 531, L8
Boogert, A. A., Gerakines, P. A., & Whittet, D. C. 2015, ARA&A, 53
Bouilloud, M., Fray, N., Bénilan, Y., et al. 2015, MNRAS, 451, 2145
Chandra, S., Eckhardt, A. K., Turner, A. M., et al. 2021, CEJ, 27, 4939
Collings, M., Dever, J. W., Fraser, H. J., et al. 2003, Ap&SS, 285, 633
d'Hendecourt, L., Allamandola, L., Baas, F., et al. 1982, A&A, 109, L12
Davey, M., Stals, E., Panis, B., et al. 2005, Anal. Biochem., 347, 201
Devlin, J. P. 1992, JPC, 96, 6185
Eckhardt, A. K., Bergantini, A., Singh, S. K., et al. 2019, AngCh, 58, 5663
Fourikis, N., Sinclair, M., Robinson, B., et al. 1974, AuJPh, 27, 425
Garrod, R. T., Widicus Weaver, S. L., & Herbst, E. 2008, ApJ, 682, 283
Gilmore, W., Morris, M., Johnson, D. R., et al. 1976, ApJ, 204, 43
Gottlieb, C. A. 1973, in Molecules in the Galactic Environment, ed. M. A. Gordon & L. E. Snyder (New York: Wiley), 181

Guan, J., Hu, Y., Zou, H., et al. 2012, JChPh, 137, 124308
He, J., Emtiaz, S., & Vidali, G. 2018, ApJ, 863, 156
Hilbig, R., & Wallenstein, R. 1982, ApOpt, 21, 913
Hovington, P., Drouin, D., & Gauvin, R. 1997, Scanning, 19, 1
Jamieson, C. S., Mebel, A. M., & Kaiser, R. I. 2006, ApJS, 163, 184
Jenniskens, P., Blake, D., Wilson, M., et al. 1995, ApJ, 455, 389
Jones, B. M., & Kaiser, R. I. 2013, JPCL, 4, 1965
Kaiser, R., Eich, G., Gabrysch, A., et al. 1997, ApJ, 484, 487
Kaiser, R. I. 2002, ChRv, 102, 1309
Keen, R. 1984, The Life and Work of Friedrich Wohler (Nordhausen: Verlag Traugott Bautz GmbH)
Kimura, K., & Osafune, K. 1975, Bull. Chem. Soc. Japan, 48, 2421
Kleimeier, N. F., Abplanalp, M. J., Johnson, R. N., et al. 2021, ApJ, 911, 24
Kleimeier, N. F., Eckhardt, A. K., & Kaiser, R. I. 2020a, ApJ, 901, 84
Kleimeier, N. F., Eckhardt, A. K., Schreiner, P. R., et al. 2020b, Chem, 6, 3385
Kondrashov, F. A., Koonin, E. V., Morgunov, I. G., et al. 2006, Biology Direct, 1, 1
Kostko, O., Belau, L., Wilson, K. R., et al. 2008, JPCA, 112, 9555
Lias, S. G. 2015, in NIST Standard Reference Database Number 69, ed. P. J. Linstrom & W. G. Mallard (Gaithersburg, MD: National Institute of Standards and Technology)
Maity, S., Kaiser, R., & Jones, B. M. 2014, ApJ, 789, 36
Mardyukov, A., Eckhardt, A. K., & Schreiner, P. R. 2020, AngCh, 59, 5577
McGuire, B. A., Shingledecker, C. N., Willis, E. R., et al. 2017, ApJL, 851, L46
McMurtry, B. M., Saito, S. E., Turner, A. M., et al. 2016a, ApJ, 831, 174
McMurtry, B. M., Turner, A. M., Saito, S. E., et al. 2016b, CP, 472, 173
Mehringer, D. M., & Snyder, L. E. 1996, ApJ, 471, 897
Mehringer, D. M., Snyder, L. E., Miao, Y., et al. 1997, ApJL, 480, L71
Morton, R. J., & Kaiser, R. I. 2003, P&SS, 51, 365
Niu, B., Shirley, D. A., & Bai, Y. 1993, JChPh, 98, 4377
Palumbo, M. E. 1997, JPCA, 101, 4298
Pearson, J., Sastry, K., Herbst, E., et al. 1997, ApJ, 480, 420
Petrik, N. G., Monckton, R. J., Koehler, S. P., et al. 2014, JChPh, 140, 204710
Sandford, S., Allamandola, L., Tielens, A., et al. 1988, ApJ, 329, 498
Sillero, M., Sillero, A., & Sols, A. 1969, Eur.J. Biochem., 10, 345
South, P. F., Walker, B. J., Cavanagh, A. P., et al. 2017, Plant Cell, 29, 808
Summermatter, S., Santos, G., Pérez-Schindler, J., et al. 2013, PNAS, 110, 8738
Tielens, A., McKee, C., Seab, C., et al. 1994, ApJ, 431, 321
Tsuge, M., Hidaka, H., Kouchi, A., et al. 2020, ApJ, 900, 187
Turner, A. M., Abplanalp, M. J., Blair, T. J., et al. 2018, ApJS, 234, 6
Turner, A. M., Abplanalp, M. J., Chen, S. Y., et al. 2015, PCCP, 17, 27281
Turner, A. M., & Kaiser, R. I. 2020, Acc. Chem. Res., 53, 2791
Turner, A. M., Koutsogiannis, A. S., Kleimeier, N. F., et al. 2020, ApJ, 896, 88
Turner, B. 1977, ApJL, 213, L75
Turner, B. E., & Apponi, A. J. 2001, ApJL, 561, L207
Vasyunin, A., & Herbst, E. 2013, ApJ, 769, 34
Vijay, D., & Sastry, G. N. 2005, JMoSt, 714, 199
von Niessen, W., Bieri, G., & Åsbrink, L. 1980, JESRP, 21, 175
Wakil, S. J. 1958, JACS, 80, 6465
Westley, M., Baragiola, R., Johnson, R., et al. 1995, Natur, 373, 405
Winnewisser, G., & Churchwell, E. 1975, ApJL, 200, L33
Woon, D. E. 2021, The Astrochymist, www.astrochymist.org
Xu, B., Stein, T., Ablikim, U., et al. 2019, FaDi, 217, 414
Zamirri, L., Casassa, S., Rimola, A., et al. 2018, MNRAS, 480, 1427
Zamirri, L., Ugliengo, P., Ceccarelli, C., et al. 2019, ESC, 3, 1499
Zheng, W., Jewitt, D., & Kaiser, R. I. 2006a, ApJ, 639, 534
Zheng, W., Jewitt, D., & Kaiser, R. I. 2006b, ApJ, 648, 753
Zheng, W., Jewitt, D., & Kaiser, R. I. 2007, CPL, 435, 289
Zhou, L., Zheng, W., Kaiser, R. I., et al. 2010, ApJ, 718, 1243
Zhu, C., Frigge, R., Bergantini, A., et al. 2019, ApJ, 881, 156
Zhu, C., Frigge, R., Turner, A. M., et al. 2018, ChCom, 54, 5716
Zhu, C., Turner, A. M., Meinert, C., et al. 2020, ApJ, 889, 134
Zuckerman, B., Ball, J. A., & Gottlieb, C. A. 1971, ApJL, 163, L41
Zuckerman, B., Turner, B., Johnson, D., et al. 1975, ApJL, 196, L99